HHS Public Access

Author manuscript

Oncogene. Author manuscript; available in PMC 2024 February 21.

Published in final edited form as:

Oncogene. 2023 August ; 42(34): 2536–2546. doi:10.1038/s41388-023-02775-7.

Pancreatic Ductal Adenocarcinoma Induces Neural Injury that Promotes a Transcriptomic and Functional Repair Signature by Peripheral Neuroglia

Jonathan Weitz[1], **Bharti Garg**[1], **Alexei Martsinkovskiy**[1], **Sandip Patel**[2], **Herve Tiriac**[1], **Andrew M. Lowy**[1]

[1]Department of Surgery, University of California, San Diego, La Jolla CA CA 92093, USA.

[2]Division of Hematology-Oncology in the Department of Medicine, University of California San Diego, La Jolla, CA 92093, USA.

Abstract

Perineural invasion (PNI) is the phenomenon whereby cancer cells invade the space surrounding nerves. PNI occurs frequently in epithelial malignancies, but is especially characteristic of pancreatic ductal adenocarcinoma (PDAC). The presence of PNI portends an increased incidence of local recurrence, metastasis and poorer overall survival. While interactions between tumor cells and nerves have been investigated, the etiology and initiating cues for PNI development is not well understood. Here, we used digital spatial profiling to reveal changes in the transcriptome and to allow for a functional analysis of neural-supportive cell types present within the tumor-nerve microenvironment of PDAC during PNI. We found that hypertrophic tumor-associated nerves within PDAC express transcriptomic signals of nerve damage including programmed cell death, Schwann cell proliferation signaling pathways, as well as macrophage clearance of apoptotic cell debris by phagocytosis. Moreover, we identified that neural hypertrophic regions have increased local neuroglial cell proliferation which was tracked using EdU tumor labeling in KPC mice, as well as frequent TUNEL positivity, suggestive of a high turnover rate. Functional calcium imaging studies using human PDAC organotypic slices confirmed nerve bundles had neuronal activity, as well as contained NGFR+ cells with high sustained calcium levels, which are indicative of apoptosis. This study reveals a common gene expression pattern that characterizes solid tumor-induced damage to local nerves. These data provide new insights into the pathobiology of the tumor-nerve microenvironment during PDAC as well as other gastrointestinal cancers.

Corresponding Authors: jweitz@health.ucsd.edu, alowy@health.ucsd.edu.

AUTHOR CONTRIBUTIONS

Conceptualization: JRW, AML
Methodology: JRW, BG, HT, SP, AML
Investigation: JRW, BG, HT, AML
Funding acquisition: JRW, AML
Writing – original draft: JRW
Writing – review & editing: JW, HT, SP, AML

COMPETING INTERESTS

The authors declare no competing financial interests.

Competing Interests statement: The authors have nothing to disclose.

INTRODUCTION

The pancreas is innervated by sensory, parasympathetic, sympathetic fibers (1–3) and receives neuronal input from enteric neurons of the gut (4). A dramatic increase in neural density is observed in pancreatic ductal adenocarcinoma (PDAC) (5, 6). During perineural invasion (PNI), PDAC cells hijack and utilize pancreatic neural networks as conduits for metastasis. These paracrine signaling interactions between nerves and pancreatic cancer cells have been shown to promote cancer cell migration (7) and proliferation (6).

The presence of PNI has been shown to be a poor prognostic factor and is estimated to be found in 70–100% of PDAC specimens (8). Currently, there are no approved treatments which target PNI. While nerve and cancer cell interactions have been the focus of most PNI research, the Schwann cell is the most abundant cell type found within nerve bundles (9). A recent report demonstrated that Schwann cells within pancreatic nerves organize into dynamic tracks that promote cancer cell migration and resemble non-myelinated repair-type Schwann cells (10). In other pathological conditions such as spinal injury, repair-Schwann cells align into Bünger bands which locally proliferate, enable axonal guidance, and promote nerve regeneration; reviewed in (11).

To better understand the functional and molecular signals regulating perineural invasion and the local tumor-nerve microenvironment, we performed digital spatial analysis to characterize changes occurring between thin caliber axon fibers, more commonly present during physiologic conditions in the pancreas, as well as larger nerve bundles, which are commonly found during PDAC. We show that large nerve bundle regions have transcriptional signatures characterized by the upregulation of BMP, MAPK and JUN signaling, as well as apoptosis. Functional analysis supporting these data were performed by proliferation (EdU) and apoptosis (TUNEL) analysis, which indicate a high turnover of local Schwann cells. This study provides further insights into the functional and molecular framework of the tumor-nerve microenvironment.

METHODS

Immunofluorescence and Confocal Imaging:

KPC tumor tissues were fixed in 4% paraformaldehyde and subsequently cryoprotected (30% sucrose). Tissue sections were cut at (40 μm) cut on a cryostat. After permeabilization (PBS–Triton X-100 0.3%), sections were incubated in blocking solution (permeabilization buffer with 1% donkey serum). Primary antibodies were diluted in blocking solution. Immunofluorescence images were aquired using confocal microscopy using a Nikon Ti microscope with integrated autofocus, automated XY and Z stage, A1R hybrid confocal scanner including a high-resolution (4096×4096) scanner, LU4 four-laser AOTF unit with 405, 488, 561, and 647 lasers, Plan Apo 10 (NA 0.8), 20X (NA 0.9) dry objectives. To visualize macrophages, we used antibodies against F4/80 (1:200, catalog number 123116; BioLegend, San Diego, CA; and 1:200 catalog number MCA497R; Bio Rad, Hercules, CA), PanCK to visualize epithelial cells (1:100, catalog number SC8018; Santa Cruz Biotechnology, Dallas, TX). Cell nuclei were stained with DAPI 1:1000 4′, 6-diamidino-2-phenylindole (DAPI) (Catalogue Number D1306; Thermo Fisher/Life

Technologies, Waltham, MA). Slides were mounted with ProLong Antifade (Thermo Fisher/Life Technologies, Waltham, MA). H&E-stained slides were used for morphologic evaluation of tumors.

GeoMx Nanostring and Bioinformatics analysis:

GeoMx® Digital Spatial Profiling (DSP) was performed using KPC mouse tissues from nerve bundles, nerve regions containing macrophages, nerve fibers, acinar, acinar tissue containing nerve fibers and spleen for a total of 23 geometric regions of interest (ROIs). Morphology markers included antibodies for tyrosine hydroxylase, F4/80, PanCK, and and Syto 83 orange DNA dye to visualize tissue morphology guiding the selection of the 23 ROIs. Differential expression analysis, PCA plots, heatmaps and gene ontology analysis was generated using the BioJupies maayanlab.cloud pipeline (12). To eliminate any enrichment bias, sequential ROIs from KPC section were not included in analysis, and only included for validation controls. For macrophage subtype classification analysis, genes with expression values with greater than +2 fold change received a value of +1, values less than −2 fold change received a score of −1, and expression value fold change where X is between $-2 < \times < 2$ received a value of 0.

Proliferation and apoptosis analysis:

KPC mice were monitored daily until a palpable tumor was discovered. 18 – 24 week old male and female KPC mice were bred to a C57/B6 background. Ethical standards were considered and followed according to the UCSD IACUC protocols. Subsequently, daily EdU injections (catalog number 900584; Sigma Aldrich, Burlington, MA) were given (50 mg/kg) until euthanasia. Tumors were removed, fixed in 4% PFA and cryoprotected in 30% sucrose. EdU was detected using the Click-iT EdU kit (Catalogue Number C10337; Thermo Fisher/Life Technologies, Waltham, MA). Colocalization analysis of confocal images of TH positive and EdU positive cells was performed using ImageJ. TUNEL positive cells in non-EdU injected mice were identified using the Click-iT Tunel kit (C10245; Thermo Fisher/Life Technologies, Waltham, MA) was used according to the manufacturer protocol. Colocalization analysis of confocal images of TH positive and TUNEL positive.

Human protein atlas tissues:

Protein analysis on human tumor sections was performed using images provided by the Human Protein Atlas (HPA) at proteinatlas.org. Representative images were selected from regions of the tumor tissue and healthy tissue from pancreas, stomach and liver containing positive staining for the antibody CAB005268.

Human Donor Tissue Information:

Donor tumor resection from patient sample ID number 278 was diagnosed with poorly differentiated invasive ductal adenocarcinoma. Staging ypT2N2. Male age 75. Patient was treated showed no treatment effect from neoadjuvant chemotherapy FOLFIRINOX. Donor consent was given and tissue was distributed by the UCSD Moores cancer center biorepository.

Calcium Imaging:

$[Ca^{2+}]_i$ imaging experiments, slices were bathed in HEPES buffered solution (125 mmol/L NaCl, 5.9 mmol/L KCl, 2.56 mmol/L CaCl2, 1 mmol/L MgCl2, 25 mmol/L HEPES, 0.1% BSA, pH 7.4) and solutions were exchanged using a peristaltic pump (Isamtec, Wertheim Germany, catalogue number ISM832C). To visualize macrophages in situ, we used fluorescence-conjugated antibodies for CD11b (1:200) (M1/70, catalog number 12–0112-82; Thermo Fischer). Nerve bundles were labeled with NGFR conjugated APC fluorophore (1:200, ME20.4 BioLegend, San Diego, CA) and co-labeled with Fluo-4, AM, cell permeant (Thermo Fisher/Life Technologies Waltham, MA, catalog number F14201) in order to track and analyze for functional analysis.

Statistical Analysis:

For nanostring studies, sample sizes for ROIs were selected based on the clearly definable total number of available bundles within the tissue sections. Raw p-values were further corrected for using FDR. Volcano plot gene fold changes were transformed using log2 and displayed on the x axis; P-values were corrected using the Benjamini-Hochberg method, transformed using –log10. For pathway enrichment analysis, significant terms are determined by using a cut-off of p-value<0.1 after applying Benjamini-Hochberg correction. In mouse studies, a large effect size was observed in our murine EdU and TUNEL studies, a small sample size adequate to determine observational changes. No randomization or blinding was needed for these studies.

Data availability:

Raw data for this study were generated at the University of California, San Diego Moores by the Sandip Patel Lab (https://moorescancercenter.ucsd.edu/research/centers-and-labs/patel-lab/index.html). Derived data supporting the findings of this study are available from the corresponding author upon request.

RESULTS

Apoptosis and JUN signaling gene signatures are upregulated within the tumor-nerve microenvironment of KPC mice.

To investigate tumor-nerve interactions which occur during PDAC, we utilized the KPC genetic mouse model, in which pancreas specific expression of oncogenic Kras and mutant p53 drives development of PDAC. Mice begin to develop pancreatic intraepithelial neoplasia (PanIN) at 8–10wks of age and disease progression to PDAC typically occurs within 16–20wks (Rhim et al., 2013). Once tumors reached 1 cm in diameter, measured by palpation, mice were sacrificed, and immunofluorescence was performed on the frozen fixed tumors using markers for nerves (TH), epithelial cells (PanCK) and macrophages (F4/80). High magnification images resolved differences in tumor associated nerve structures where axon fibers and larger caliber bundles could be found (Figure 1A). The labeled cryosections were loaded onto the GeoMx nanostring instrument and a representative diagram of the pipeline is shown (Figure 1B). Regions of interest (ROI) were collected from the tumor tissue and barcoded by the instrument in a plate for next generation sequence analysis.

Principal component analysis was performed on 10 ROIs containing either axon fibers, or larger nerve bundles (Figure 1C). We found that larger nerve bundles clustered together (red), while axonal ROIs clustered separately (blue). A heatmap was generated from the expression values, which revealed two large distinct clusters which separated the axonal gene signatures from the nerve bundle gene signatures. To note, axon # 81 ROI, clustered more closely with the nerve bundle ROIs (Figure 1D). Differential expression analysis was performed, and a volcano plot (Figure 1E, top) was created to show the most significant upregulated and downregulated genes in nerve bundles, as well as an MA plot to show the amplitude of expression (Figure 1E, bottom). Amongst the most upregulated genes included *BMP4*, *BMP7* and *BDNF*. Gene ontology analysis was performed, which revealed upregulation of numerous pathways related to MAPK, JUN kinase, as well as apoptosis gene signatures (Figure 1F). Based on the GO gene signatures, we selected genes from pathways enriched for apoptosis, JUN kinase, as well as SMAD/BMP signaling, which was highly upregulated in Kegg Pathways (Figure 1G). Interestingly *MT2* was the most downregulated gene in large nerve bundles: it has shown to be highly expressed in healthy nerves, but not in painful neuromas (13), and is lost during chemotherapy induced neuropathic pain (14). These results reveal a unique transcriptional program in cancer associated nerve bundles marked by upregulation of MAPK, apoptosis and JUN gene signatures. This molecular signature has been observed in Schwann cell regeneration, in non-cancer contexts (15, 16). As a check for the fidelity of our analysis, we performed internal controls comparing spleen, acinar tissues (Supplemental Figure 1) and sequential regions in tumor tissues, compared to non-paired regions (Supplemental Figure 2). Regions of acinar tissues and spleen showed independent clustering and enrichment for genes involved in pancreatic digestion. Additionally, sequentially matched regions clustered together using PCA analysis. Lastly, the top differentially expressed genes in our data provide insight into tissue type differences that were resolved by nanostring analysis (TH+ fibers, bundles, spleen, and acinar) (Supplemental Table 1 and Table 2). Quality control of the data analyzed revealed high quality UMIQ30 values, as well as read correlations with nuclei counts (Supplemental Figure 3). Taken together, these molecular data indicate a nerve repair program is activated by repair Schwann cells in PDAC associated nerves.

Nerve associated macrophage express signatures reflective of a role in phagocytosis.

Tissue resident macrophages have unique functions based on their origin and tissue location. For instance, cardiac resident macrophages participate in electoral conduction via gap junction communication with cardiac myocytes (17). While numerous reports have described tumor associated macrophages (TAMs) to function as pro- or anti tumorigenic (18–20), only a few studies have been reported on the function of endoneurial macrophages within PDAC. In these studies, nerve associated macrophages (NAMs) have been shown to secrete neurotrophic factors (21), as well as express inflammatory regulators such as LIF and CTSB (22, 23). However, to our knowledge a molecular characterization of local macrophages *in-situ* has not been performed. Here we performed digital spatial sequencing analysis of PDAC nerve bundles in regions devoid of- or containing F4/80+ macrophages (Figure 2A–2B). Principal component analysis revealed distinct clustering of bundles with and without macrophages (Figure 2C). Differential expression showed an enrichment for macrophage type associated genes including *Csf1r*, *Cd68* and *AIF1*, enriched

in F4/80+ bundles and did not contain upregulated epithelial or fibroblast signatures (Figure 2D). The genes *Csf1r, and AIF1* which are frequently expressed in macrophages were significantly upregulated (p = .049 for *Csf1r* and p = .043 for *AIF1;* students t-test). Differential expression analysis was performed, and a volcano plot (Figure 2E, top) was created to reveal the most significantly upregulated and downregulated genes in nerve bundles, as well as an MA plot to show the amplitude of expression (Figure 2E, bottom). Amongst the most upregulated genes included *Marcks* and *Fcgr2b, and Psap*. Gene ontology analysis revealed upregulation of pathways involved in antigen presentation, phagocytosis and lysosome compartments (Figure 2F). Based on the GO gene signatures enriched in Kegg Pathways, we highlighted selected genes from enriched pathways for apoptosis, as well as chemokine ligands/receptors and TAM receptor/ligands, which play pivotal roles in macrophage function (Figure 2G). We found that *CCL7, Cxcl12* and *Cxcl13* were amongst the most differentially expressed genes enriched in 5 TH+, F4/80+ ROIs. Interestingly, the aforementioned chemokines have been shown to be important for macrophage chemotaxis to damaged nerves (CCL7) (24, 25), and neuropathic pain (Cxcl12, Cxcl13) (26, 27). To note, many interleukin genes were not included as they were detected at low frequency (Supplemental Table 3). These transcriptomic signatures strongly suggest that local F4/80+ macrophages within nerve bundles have phagocytic function. To further molecularly classify nerve associated macrophages, we performed an enrichment scoring of macrophages genes identified in various TAM-types known to be present in the tumor microenvironment (19). In this analysis, we found that nerve associated macrophages share some features with lipid-associated TAMs (Supplemental Figure 4). While their role in PDAC biology has not been described, in the context of nerve injury, nerve associated macrophages have been shown to play a key role in phagocytosis, antigen presentation and clearance of damaged axons during Wallerian degeneration (28).

Local neuroglia proliferate within the tumor nerve microenvironment.

Our findings that transcriptomic signatures of non-myelinating repair-type Schwann cells (*BMPs*, *JUN* kinases and *BDNF*) are upregulated in PDAC associated nerve bundles along with nerve-associated macrophage upregulation of phagocytic gene signatures, resembles changes found in damaged nerves during traumatic non-cancer related injuries. In such settings, neuroglial (neural supportive cell types; macrophages, Schwann cells) undergo a functional transformation and proliferate locally to support the repair and regeneration of a damaged axons (29–31). As neuronal cells bodies are largely absent, while their specialized axonal processes extend into the peripheral nervous system, we hypothesized that during PDAC, local neuroglial, would actively proliferate at sites of nerve damage. To test this, when a palpable tumor was detected, we enrolled mice into daily intraperitoneal injections of EdU (50 mg/kg), which allowed tracking of cell proliferation over multiple days. We performed colocalization analysis in TH+ nerves, in acinar regions (remote from the tumor) as well as intra-tumoral TH+ nerve bundles. We found in non-tumor tissues, nerve fibers did not colocalize with EdU+ nuclei (DAPI) independent of neural density, while in intra-tumoral regions EdU+ nuclei were found within TH+ bundles (Figure 3A–3E). Split channel images confirmed presence of nuclei colocalization (Supplemental Figure 5). Proliferative nuclei were quantified and were significantly increased in TH+ regions within tumors compared to TH+ regions in acinar tissues, which we did not detect in our analysis

(Figure 3F). These results indicate that neuroglial have functional responses (increased proliferation), based on their proximity to a growing tumor. Given that paracrine signaling factors secreted by the pancreatic cancer TME, such as LIF, SLIT2, and NGF (5, 22, 32), have been shown to promote Schwann cell proliferation *in-vitro*, we sought to determine whether increased proliferation rates were found in nearby epithelial cells (less than 50 microns), compared to distant TH+ bundles (greater than 50 microns). After stratification of intra-tumor TH staining into near epithelial or distant epithelial cells (PanCK+), we did not find a significant difference in TH+, EdU+ nerves based on tumor cell location (Figure 3G–3I). These data indicate that the proliferative phenotype of local neuroglia in the setting of the tumor-nerve microenvironment does not require direct contact with epithelial cells.

The tumor nerve microenvironment of human PDAC and other gastrointestinal malignancies express markers of non-myelinating Schwann cell phenotypes.

Given our functional and transcriptomic data in our mouse models, we sought to identify how the transcriptional state of Schwann cells differs in 'healthy' acinar tissue and within pancreatic tumors. As we identified transcriptional and functional gene signatures of non-myelinating repair Schwann cells within tumor tissues, we hypothesized that adjacent healthy acinar tissue enriched for TH+ axons would have gene signatures of Schwann cells, which did not present a de-differentiated, non-myelinating phenotype. As such, we compared core Schwann single cell transcriptomic signatures defined by Panglao DB, as well as non-myelinating Schwann cells defined by OnClass (CL:0002376), and previously published characterized in PDAC (10, 33). In regions containing TH+ staining independently of tumor location (acinar, TH+ fibers, TH+ Bundles), we identified core Schwann cell transcriptomic signatures (*Cryab*, *MPZ*, *GFAP*) in all locations, however only in tumor TH+ regions (TH+ fibers, and bundles), did we identify enriched gene sets characteristic of non-myelinating Schwann cells (15/19 genes in bundles and 17/19 genes in axons) (Figure 4A). Notably, acinar genes were also highly enriched in acinar regions (Figure 4A; right panel). No genes were removed from OnClass (CL:0002376) signatures in our comparative analysis, however, 6 genes did not meet the minimum threshold of detection for analysis. Using gene ontology analysis, we compared axons in healthy and tumor regions and identified enrichment scores involved in spinal cord injury and complement pathway activation (Figure 4B). To functionally investigate whether cell death may be occurring within TH+ nerves, we performed TUNEL analysis which labels apoptotic cells. In some nerve bundles we identified up to 40 percent of the nuclei to be TUNEL positive, with an average of nearly 25 percent TUNEL positivity rate in tumor associated nerves from KPC mice (Supplemental Figure 6). As functional and gene ontology data revealed pathways occurring upon activation of damaged nerves, we hypothesized that a common pathway might be present across multiple tumor models, whereby tumors damage nerves, and promote a non-myelinating Schwann cell transcriptional program (Figures 4C–4D). To investigate whether this phenotype was present across multiple tumor types, we utilized the human protein atlas to interrogate the tumor-nerve microenvironment across multiple organs and tumor types. Using protein markers c-JUN and JUND which control the repair-Schwann cell phenotype (11, 16), we sought to determine whether these transcription factors were upregulated within PDAC nerve bundles compared to healthy tissues. Using the JUND antibody CAB005628, we identified low protein expression in the normal pancreas (Figure

4E) while high expression was present in nerve bundles from PDAC (Figure 4F–4G). These results were highly concordant to nerve bundles found during stomach cancer, and liver cancer (Figure 4H–4L). To confirm whether central regulators of apoptosis gene signatures were present in human tissues, we performed BCL-2 immunostaining using human PDAC specimens (Supplemental Figure 7). While, perineural invasion has been reported in many tumor types; reviewed in (34), our data suggest repair-Schwann cells and JUN kinase upregulation in nerve bundles are present across multiple tumor types, and identifies it as a cardinal feature of perineural invasion.

In-situ cytolabeling of organotypic tumor slices prepared from PDAC patients allows for functional imaging of the human tumor nerve microenvironment.

Given that we uncovered neural injury genetic signatures, as well as our TUNEL positive neuroglia in KPC mice, we sought to identify if nerve dysfunctional signatures identified within KPC models were found in human PDAC tissues. As such, we adapted an organotypic slice culture model which allows for functional Ca^{2+} imaging of nerves and immune cells of the human and mouse pancreas (35). The model required cutting of living tumor resections of de-identified human PDAC tissues (for donor information; see materials and methods) using a vibratome to produce tumor slices and loading them with the calcium indicator dye Fluo-4 (Figure 5A–5C). Utilizing *in-situ* cytolabeling with the cell surface receptor antibody NGFR, which has previously been shown to be expressed in human PDAC tumor nerve bundles (36) we identified regions of nerve bundles in human PDAC tumors (Figure 5D). We identified NGFR+ cells, as well as CD11b+ macrophages inside and near the TMNE (Figure 5E–5H). Functional imaging revealed that Ca^{2+} levels within axons of bundles can respond to cellular depolarization via potassium chloride (KCl: 25 mM). While not all cells responded, we did observe local macrophage responses which peaked shortly after KCl stimulation, indicative of a paracrine signaling response, as macrophages cannot be depolarized via KCl (Figure 5K). Interestingly we also found spontaneous activity within regions of the nerve bundle as well as NGFR+, Fluo-4+ cells which had high sustained levels of calcium (Figure 5L–5N; Supplemental Movie 1). Raw traces of live cell imaging confirmed elevated calcium levels (Figure 5O). High sustained high levels of intracellular calcium induce calcium flux into the nucleus inducing apoptosis (37). Here we show a novel technique to study the TMNE *in-situ*, as well as proof of principal functional analysis of human tissues. As pancreatic tumor slices have been kept alive for multiple days (38, 39), this adaptation of the tissue slice model for TMNE imaging will better allow for the future testing of human Schwann cell function, as well as therapeutic intervention.

DISCUSSION

Pancreatic ductal adenocarcinoma (PDAC) has the highest mortality rate of all major cancers and is currently the third leading cause of cancer-related deaths. Survival rates have minimally improved in the last 40 years, with the current five-year survival rate at 11% (40). The failure of current therapeutic approaches has been attributed to many features of PDAC including its inherent drug resistance, poor immunogenicity, and a highly immunosuppressive microenvironment associated with high rates of perineural invasion (PNI; estimated 70–100%) (8, 34). Some emerging strategies for PDAC therapy have

focused on altering these physiological features to improve therapeutic efficacy. While perineural invasion is a hallmark of PDAC (41, 42) the etiology and molecular profile of the tumor nerve microenvironment is still not known. Functional studies investigating tumor-nerve interactions began nearly 70 years ago where Levi-Montalcini and colleagues showed that different tumor types were capable of inducing nerve growth. These co-culture experiments led to the discovery of the first neural growth factor NGF, reviewed in (43). More recent studies have utilized co-cultures of dorsal root ganglion with pancreatic cancer cells to reveal effects on cancer cell tumorigenesis (44) invasion (9), as well as growth and proliferation (6, 45). To better understand the native interactions of cells within the complex PDAC tumor microenvironment, an approach that studies a spontaneous intact tumor is advantageous. As such, we utilized digital spatial transcriptomics to characterize PDAC neural bundles in the context of the KPC model and performed proliferation analysis of local Schwann cells *in-situ*.

Our findings corroborate a recent report which demonstrated that neural bundles found with PDAC tissues are enriched with Schwann cells that have been transcriptionally reprogrammed within the tumor-nerve microenvironment (10, 33). During non-cancer related traumatic nerve injury, genetic signatures (JUN kinase, BMP, MAPK), and functional signatures (neuroglial proliferation, and organization into longitudinal tracks) are indicative of neuronal damage (24, 46, 47). Multiple groups have reported that enlarged neural bundles occur more frequently near the tumor periphery, with fewer bundles occurring in the tumor core (48, 49). Interestingly, we observed proliferation of neuroglia neighboring as well as distant from epithelial cells within the pancreatic tumor. As proliferative neuroglia are a hallmark feature of neuronal injury (11, 29, 50), these data may indicate that physical damage by solid tumor stress might be imparted by cancer cells themselves or the tumor stromal components such as CAFs and the extracellular matrix. Additionally, we found a high frequency of TUNEL positive Schwann cells within nerve bundles as well, indicating increased cell death. As such, high turnover rates of Schwann cell proliferation and cell death likely influence the size of of PDAC nerve bundles and may control where, and if, the bundle remains intact. Future studies investigating the paracrine chemical (chemokines and neurotrophic factors) and physical (tumor stiffness) features that regulate this process may provide further clarity as to the etiology of perineural invasion.

Notwithstanding, our work has some limitations. While perineural invasion and hypertrophic nerve bundles are found in most cases of PDAC, the tumor-nerve microenvironment is a relatively small physical area (compared to epithelial and stromal components), which requires large tissue fragments to visualize an adequate amount of nerve bundles. To enrich for nerve bundles, we identified KPC tissues with relatively abundant nerve densities to acquire enough cell material for sequencing analysis. Along these lines, the GeoMx digital profiler has tissue size constraints to fit into the imaging window. Due to the large tissue area needed to find nerve bundles, even in KPC mice with substantial PNI, performing digital spatial sequencing on small biopsies containing multiple donors is technically very challenging. While our analyses were performed on sequential KPC tumor slices, to assure the robustness and fidelity of our data we acquired multiple regions of tumor and non-tumor tissues (spleen, acinar), to accurately perform data analysis with appropriate controls. Another limitation is that EdU labeling experiments cannot be replicated in PDAC patients.

Given that murine EdU labeling over multiple days results in accumulation of proliferation events compared to single time point at which Ki67 labels cells, we expect only rare proliferation events in humans would be observed. As such human and mouse proliferation data were not compared.

Collectively, our data indicate that peripheral nerve damage occurs during PDAC, findings which are highly concordant with other recent reports (10). Similar transcriptional gene signatures identified in our models were found within human PDAC tissues (JUN signaling pathways). To explore whether these molecular changes were associated with functional signatures, we performed live cell imaging of human PDAC tumor resections. Here we performed an organotypic slice technique, derived from previous studies exploring sensory nerves of the mouse pancreas (35), in order to study human cancer conditions. This is first model to our knowledge which allows for the functional interrogation of the human TMNE *in-situ*. Here using calcium signaling from NGFR+ labeled neuroglia as well as CD11b+ endoneurial macrophages we determined that nerve bundles have functional Ca^{2+} activity, however we found numerous NGFR+ cells had sustained high levels of calcium, which are indicative of cellular apoptosis (37). These findings indicate that a common pathway supports the response to neural injury.

While TME induced neural injury appears to underpin a key role in the etiology of hypertrophic nerve bundles, many questions remain regarding the initiating signals of PNI that account for the different rates of PNI across different tumor types (i.e., high in PDAC, while lower in other tumor types) (34). Future studies should investigate where (adjacent acinar, tumor periphery, or tumor core), and whether neurotransmission is disrupted by the growing tumor, as modulation of neural activity via vagal stimulation has been proposed as an experimental approach to the treatment of advanced disease (6, 51). It will also be of interest to study therapies that target specific branches of the autonomic nervous system (sensory, parasympathetic, and sympathetic) as they have been shown to have distinct functions in the TME, and to effect survival in murine PDAC models (52, 53).

Supplementary Material

Refer to Web version on PubMed Central for supplementary material.

ACKNOWLEDGEMENTS

Funding: This work was supported by a grant from the National Cancer Institute, 1F32CA265052–01 (JRW). Confocal imaging and histology core was done with support from the UCSD Specialized Cancer Support Center P30 grant 2P30CA023100. We would like to thank Chandra Inglis and Karthik Ramesh from the Patel lab for their expert assistance in using the GeoMx Nanostring instrument and bioinformatics processing.

REFERENCES

1. Rodriguez-Diaz R, Abdulreda MH, Formoso AL, Gans I, Ricordi C, Berggren PO, et al. Innervation patterns of autonomic axons in the human endocrine pancreas. Cell Metab. 2011;14(1):45–54. doi: 10.1016/j.cmet.2011.05.008. [PubMed: 21723503]
2. Chien HJ, Chiang TC, Peng SJ, Chung MH, Chou YH, Lee CY, et al. Human pancreatic afferent and efferent nerves: mapping and 3-D illustration of exocrine, endocrine, and adipose innervation.

Am J Physiol Gastrointest Liver Physiol. 2019;317(5):G694–G706. doi: 10.1152/ajpgi.00116.2019. [PubMed: 31509431]

3. Borden P, Houtz J, Leach SD, Kuruvilla R. Sympathetic innervation during development is necessary for pancreatic islet architecture and functional maturation. Cell Rep. 2013;4(2):287–301. doi: 10.1016/j.celrep.2013.06.019. [PubMed: 23850289]
4. Kirchgessner AL, Gershon MD. Innervation of the pancreas by neurons in the gut. J Neurosci. 1990;10(5):1626–42. doi: 10.1523/JNEUROSCI.10-05-01626.1990. [PubMed: 2159059]
5. Ceyhan GO, Bergmann F, Kadihasanoglu M, Altintas B, Demir IE, Hinz U, et al. Pancreatic neuropathy and neuropathic pain--a comprehensive pathomorphological study of 546 cases. Gastroenterology. 2009;136(1):177–86 e1. doi: 10.1053/j.gastro.2008.09.029. [PubMed: 18992743]
6. Renz BW, Takahashi R, Tanaka T, Macchini M, Hayakawa Y, Dantes Z, et al. beta2 Adrenergic-Neurotrophin Feedforward Loop Promotes Pancreatic Cancer. Cancer Cell. 2018;33(1):75–90 e7. doi: 10.1016/j.ccell.2017.11.007. [PubMed: 29249692]
7. Amit M, Na'ara S, Leider-Trejo L, Binenbaum Y, Kulish N, Fridman E, et al. Upregulation of RET induces perineurial invasion of pancreatic adenocarcinoma. Oncogene. 2017;36(23):3232–9. doi: 10.1038/onc.2016.483. [PubMed: 28092668]
8. Liebl F, Demir IE, Mayer K, Schuster T, D'Haese JG, Becker K, et al. The impact of neural invasion severity in gastrointestinal malignancies: a clinicopathological study. Ann Surg. 2014;260(5):900–7; discussion 7–8. doi: 10.1097/SLA.0000000000000968. [PubMed: 25379860]
9. Deborde S, Omelchenko T, Lyubchik A, Zhou Y, He S, McNamara WF, et al. Schwann cells induce cancer cell dispersion and invasion. J Clin Invest. 2016;126(4):1538–54. doi: 10.1172/JCI82658. [PubMed: 26999607]
10. Deborde S, Gusain L, Powers A, Marcadis A, Yu Y, Chen CH, et al. Reprogrammed Schwann Cells Organize into Dynamic Tracks that Promote Pancreatic Cancer Invasion. Cancer Discov. 2022;12(10):2454–73. doi: 10.1158/2159-8290.CD-21-1690. [PubMed: 35881881]
11. Jessen KR, Mirsky R. The repair Schwann cell and its function in regenerating nerves. J Physiol. 2016;594(13):3521–31. Epub 20160321. doi: 10.1113/JP270874. [PubMed: 26864683]
12. Torre D, Lachmann A, Ma'ayan A. BioJupies: Automated Generation of Interactive Notebooks for RNA-Seq Data Analysis in the Cloud. Cell Syst. 2018;7(5):556–61.e3. Epub 20181114. doi: 10.1016/j.cels.2018.10.007. [PubMed: 30447998]
13. Oki G, Wada T, Iba K, Aiki H, Sasaki K, Imai SI, et al. Metallothionein deficiency in the injured peripheral nerves of complex regional pain syndrome as revealed by proteomics. Pain. 2012;153(3):532–9. Epub 20120116. doi: 10.1016/j.pain.2011.11.008. [PubMed: 22249007]
14. Huang X, Deng J, Xu T, Xin W, Zhang Y, Ruan X. Downregulation of metallothionein-2 contributes to oxaliplatin-induced neuropathic pain. J Neuroinflammation. 2021;18(1):91. doi: 10.1186/s12974-021-02139-6. [PubMed: 33849565]
15. Wei Z, Shu S, Zhang M, Xie S, Tang S, Nie K, et al. A Subpopulation of Schwann Cell-Like Cells With Nerve Regeneration Signatures Is Identified Through Single-Cell RNA Sequencing. Front Physiol. 2021;12:637924. Epub 20210510. doi: 10.3389/fphys.2021.637924. [PubMed: 34093220]
16. Arthur-Farraj PJ, Latouche M, Wilton DK, Quintes S, Chabrol E, Banerjee A, et al. c-Jun reprograms Schwann cells of injured nerves to generate a repair cell essential for regeneration. Neuron. 2012;75(4):633–47. doi: 10.1016/j.neuron.2012.06.021. [PubMed: 22920255]
17. Hulsmans M, Clauss S, Xiao L, Aguirre AD, King KR, Hanley A, et al. Macrophages Facilitate Electrical Conduction in the Heart. Cell. 2017;169(3):510–22.e20. doi: 10.1016/j.cell.2017.03.050. [PubMed: 28431249]
18. Pittet MJ, Michielin O, Migliorini D. Clinical relevance of tumour-associated macrophages. Nat Rev Clin Oncol. 2022;19(6):402–21. Epub 20220330. doi: 10.1038/s41571-022-00620-6. [PubMed: 35354979]
19. Ma RY, Black A, Qian BZ. Macrophage diversity in cancer revisited in the era of single-cell omics. Trends Immunol. 2022;43(7):546–63. Epub 20220609. doi: 10.1016/j.it.2022.04.008. [PubMed: 35690521]
20. Lubitz GS, Brody JD. Not just neighbours: positive feedback between tumour-associated macrophages and exhausted T cells. Nat Rev Immunol. 2022;22(1):3. doi: 10.1038/s41577-021-00660-6. [PubMed: 34789868]

21. Cavel O, Shomron O, Shabtay A, Vital J, Trejo-Leider L, Weizman N, et al. Endoneurial macrophages induce perineural invasion of pancreatic cancer cells by secretion of GDNF and activation of RET tyrosine kinase receptor. Cancer Res. 2012;72(22):5733–43. Epub 20120912. doi: 10.1158/0008-5472.CAN-12-0764. [PubMed: 22971345]
22. Bressy C, Lac S, Nigri J, Leca J, Roques J, Lavaut MN, et al. LIF Drives Neural Remodeling in Pancreatic Cancer and Offers a New Candidate Biomarker. Cancer Res. 2018;78(4):909–21. doi: 10.1158/0008-5472.CAN-15-2790. [PubMed: 29269518]
23. Bakst RL, Xiong H, Chen CH, Deborde S, Lyubchik A, Zhou Y, et al. Inflammatory Monocytes Promote Perineural Invasion via CCL2-Mediated Recruitment and Cathepsin B Expression. Cancer Res. 2017;77(22):6400–14. Epub 20170926. doi: 10.1158/0008-5472.CAN-17-1612. [PubMed: 28951461]
24. Ydens E, Amann L, Asselbergh B, Scott CL, Martens L, Sichien D, et al. Profiling peripheral nerve macrophages reveals two macrophage subsets with distinct localization, transcriptome and response to injury. Nat Neurosci. 2020;23(5):676–89. doi: 10.1038/s41593-020-0618-6. [PubMed: 32284604]
25. Xuan W, Qu Q, Zheng B, Xiong S, Fan GH. The chemotaxis of M1 and M2 macrophages is regulated by different chemokines. J Leukoc Biol. 2015;97(1):61–9. doi: 10.1189/jlb.1A0314-170R. [PubMed: 25359998]
26. Yu Y, Huang X, Di Y, Qu L, Fan N. Effect of CXCL12/CXCR4 signaling on neuropathic pain after chronic compression of dorsal root ganglion. Sci Rep. 2017;7(1):5707. doi: 10.1038/s41598-017-05954-1. [PubMed: 28720830]
27. Jiang BC, Cao DL, Zhang X, Zhang ZJ, He LN, Li CH, et al. CXCL13 drives spinal astrocyte activation and neuropathic pain via CXCR5. J Clin Invest. 2016;126(2):745–61. doi: 10.1172/JCI81950. [PubMed: 26752644]
28. Chen P, Piao X, Bonaldo P. Role of macrophages in Wallerian degeneration and axonal regeneration after peripheral nerve injury. Acta Neuropathol. 2015;130(5):605–18. doi: 10.1007/s00401-015-1482-4. [PubMed: 26419777]
29. Parfejevs V, Debbache J, Shakhova O, Schaefer SM, Glausch M, Wegner M, et al. Injury-activated glial cells promote wound healing of the adult skin in mice. Nat Commun. 2018;9(1):236. Epub 20180116. doi: 10.1038/s41467-017-01488-2. [PubMed: 29339718]
30. Avraham O, Feng R, Ewan EE, Rustenhoven J, Zhao G, Cavalli V. Profiling sensory neuron microenvironment after peripheral and central axon injury reveals key pathways for neural repair. Elife. 2021;10. Epub 20210929. doi: 10.7554/eLife.68457.
31. Jessen KR, Mirsky R. Negative regulation of myelination: relevance for development, injury, and demyelinating disease. Glia. 2008;56(14):1552–65. doi: 10.1002/glia.20761. [PubMed: 18803323]
32. Secq V, Leca J, Bressy C, Guillaumond F, Skrobuk P, Nigri J, et al. Stromal SLIT2 impacts on pancreatic cancer-associated neural remodeling. Cell Death Dis. 2015;6(1):e1592. doi: 10.1038/cddis.2014.557. [PubMed: 25590802]
33. Sun C, Ye Y, Tan Z, Liu Y, Li Y, Hu W, et al. Tumor-associated nonmyelinating Schwann cell-expressed PVT1 promotes pancreatic cancer kynurenine pathway and tumor immune exclusion. Sci Adv. 2023;9(5):eadd6995. doi: 10.1126/sciadv.add6995. [PubMed: 36724291]
34. Chen SH, Zhang BY, Zhou B, Zhu CZ, Sun LQ, Feng YJ. Perineural invasion of cancer: a complex crosstalk between cells and molecules in the perineural niche. Am J Cancer Res. 2019;9(1):1–21. Epub 20190101. [PubMed: 30755808]
35. Makhmutova M, Weitz J, Tamayo A, Pereira E, Boulina M, Almaça J, et al. Pancreatic β-Cells Communicate With Vagal Sensory Neurons. Gastroenterology. 2021;160(3):875–88.e11. Epub 20201026. doi: 10.1053/j.gastro.2020.10.034. [PubMed: 33121946]
36. Wang W, Zhao H, Zhang S, Kang E, Chen Y, Ni C, et al. Patterns of expression and function of the p75(NGFR) protein in pancreatic cancer cells and tumours. Eur J Surg Oncol. 2009;35(8):826–32. Epub 20081128. doi: 10.1016/j.ejso.2008.10.013. [PubMed: 19041213]
37. Harr MW, Distelhorst CW. Apoptosis and autophagy: decoding calcium signals that mediate life or death. Cold Spring Harb Perspect Biol. 2010;2(10):a005579. Epub 20100908. doi: 10.1101/cshperspect.a005579. [PubMed: 20826549]

38. Weitz JR, Tiriac H, Hurtado de Mendoza T, Wascher A, Lowy AM. Using Organotypic Tissue Slices to Investigate the Microenvironment of Pancreatic Cancer: Pharmacotyping and Beyond. Cancers (Basel). 2021;13(19). Epub 20211005. doi: 10.3390/cancers13194991.
39. Lim CY, Chang JH, Lee WS, Lee KM, Yoon YC, Kim J, et al. Organotypic slice cultures of pancreatic ductal adenocarcinoma preserve the tumor microenvironment and provide a platform for drug response. Pancreatology. 2018;18(8):913–27. Epub 20180926. doi: 10.1016/j.pan.2018.09.009. [PubMed: 30292644]
40. Siegel RL, Miller KD, Fuchs HE, Jemal A. Cancer statistics, 2022. CA Cancer J Clin. 2022;72(1):7–33. doi: 10.3322/caac.21708. [PubMed: 35020204]
41. Zeng L, Guo Y, Liang J, Chen S, Peng P, Zhang Q, et al. Perineural Invasion and TAMs in Pancreatic Ductal Adenocarcinomas: Review of the Original Pathology Reports Using Immunohistochemical Enhancement and Relationships with Clinicopathological Features. J Cancer. 2014;5(9):754–60. doi: 10.7150/jca.10238. [PubMed: 25368675]
42. Habtezion A, Edderkaoui M, Pandol SJ. Macrophages and pancreatic ductal adenocarcinoma. Cancer Lett. 2016;381(1):211–6. doi: 10.1016/j.canlet.2015.11.049. [PubMed: 26708507]
43. Cowan WM. Viktor Hamburger and Rita Levi-Montalcini: the path to the discovery of nerve growth factor. Annu Rev Neurosci. 2001;24:551–600. doi: 10.1146/annurev.neuro.24.1.551. [PubMed: 11283321]
44. Sinha S, Fu YY, Grimont A, Ketcham M, Lafaro K, Saglimbeni JA, et al. PanIN Neuroendocrine Cells Promote Tumorigenesis via Neuronal Cross-talk. Cancer Res. 2017;77(8):1868–79. Epub 20170406. doi: 10.1158/0008-5472.CAN-16-0899-T. [PubMed: 28386018]
45. Banh RS, Biancur DE, Yamamoto K, Sohn ASW, Walters B, Kuljanin M, et al. Neurons Release Serine to Support mRNA Translation in Pancreatic Cancer. Cell. 2020;183(5):1202–18.e25. Epub 20201102. doi: 10.1016/j.cell.2020.10.016. [PubMed: 33142117]
46. Weiss T, Taschner-Mandl S, Bileck A, Slany A, Kromp F, Rifatbegovic F, et al. Proteomics and transcriptomics of peripheral nerve tissue and cells unravel new aspects of the human Schwann cell repair phenotype. Glia. 2016;64(12):2133–53. Epub 20160822. doi: 10.1002/glia.23045. [PubMed: 27545331]
47. Brosius Lutz A, Lucas TA, Carson GA, Caneda C, Zhou L, Barres BA, et al. An RNA-sequencing transcriptome of the rodent Schwann cell response to peripheral nerve injury. J Neuroinflammation. 2022;19(1):105. Epub 20220430. doi: 10.1186/s12974-022-02462-6. [PubMed: 35501870]
48. Iwasaki T, Hiraoka N, Ino Y, Nakajima K, Kishi Y, Nara S, et al. Reduction of intrapancreatic neural density in cancer tissue predicts poorer outcome in pancreatic ductal carcinoma. Cancer Sci. 2019;110(4):1491–502. Epub 20190319. doi: 10.1111/cas.13975. [PubMed: 30776178]
49. Ceyhan GO, Bergmann F, Kadihasanoglu M, Altintas B, Demir IE, Hinz U, et al. Pancreatic neuropathy and neuropathic pain--a comprehensive pathomorphological study of 546 cases. Gastroenterology. 2009;136(1):177–86.e1. Epub 20080925. doi: 10.1053/j.gastro.2008.09.029. [PubMed: 18992743]
50. Jessen KR, Mirsky R, Lloyd AC. Schwann Cells: Development and Role in Nerve Repair. Cold Spring Harb Perspect Biol. 2015;7(7):a020487. Epub 20150508. doi: 10.1101/cshperspect.a020487. [PubMed: 25957303]
51. De Couck M, Marechal R, Moorthamers S, Van Laethem JL, Gidron Y. Vagal nerve activity predicts overall survival in metastatic pancreatic cancer, mediated by inflammation. Cancer Epidemiol. 2016;40:47–51. doi: 10.1016/j.canep.2015.11.007. [PubMed: 26618335]
52. Partecke LI, Kading A, Trung DN, Diedrich S, Sendler M, Weiss F, et al. Subdiaphragmatic vagotomy promotes tumor growth and reduces survival via TNFalpha in a murine pancreatic cancer model. Oncotarget. 2017;8(14):22501–12. doi: 10.18632/oncotarget.15019. [PubMed: 28160574]
53. Saloman JL, Albers KM, Li D, Hartman DJ, Crawford HC, Muha EA, et al. Ablation of sensory neurons in a genetic model of pancreatic ductal adenocarcinoma slows initiation and progression of cancer. Proc Natl Acad Sci U S A. 2016;113(11):3078–83. doi: 10.1073/pnas.1512603113. [PubMed: 26929329]

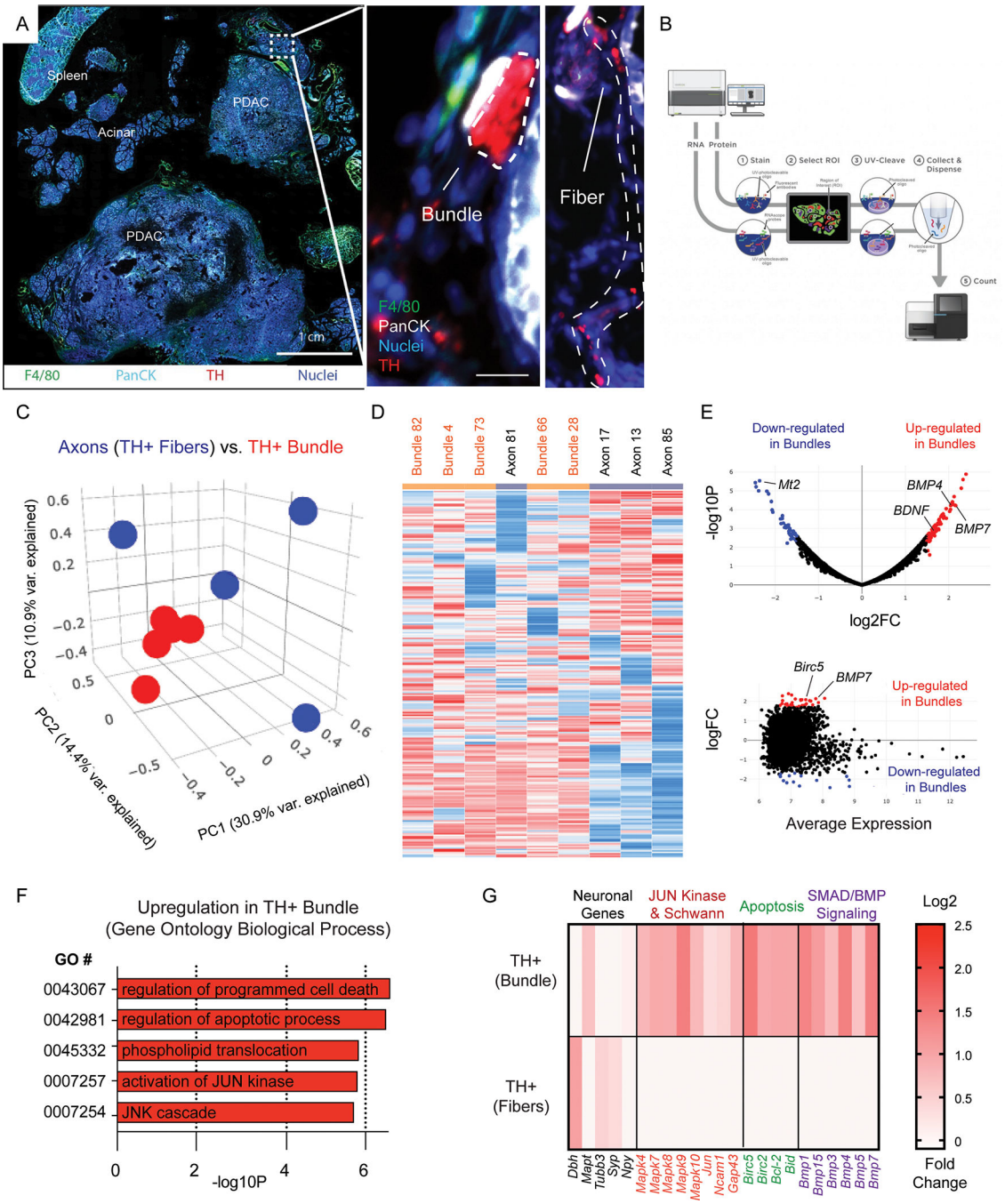

Figure 1. Digital spatial profiling of the tumor-nerve microenvironment in KPC mice reveals transcriptomic upregulation of apoptotic processes and JUN signaling gene signatures.

(A) Immunofluorescence of a whole mount tissue section containing PDAC tumor tissue, adjacent acinar tissue and spleen. Nuclei (blue), F4/80 (green), PanCK (teal), tyrosine hydroxylase (TH; red). Scale bar (1 cm, bottom right). High magnification of boxed region highlighted in A showing TH+ axonal fibers, as well as TH+ bundles (red, right panel). (B) Representative scheme of Nanostring's GeoMx digital spatial analysis pipeline. (C) Principal component analysis of comparing TH+ axonal fibers and larger caliber TH+ bundles. 9 total ROI's from N = 5 independent bundles and N = 4 axonal fibers. (D)

Hierarchical sample clustering based on differential gene expression matrix of transcription profile on individually isolated TH+ axons fibers and TH+ bundles. (E) Volcano plot and MA plot highlighting significant differential gene expression upregulated (red) and downregulated (blue) in TH+ bundles, as well as the average expression. (F) Gene ontology clustering of the most upregulated pathways based on differential gene expression analysis. (G) Highlighted gene expression changes in gene classes involved in GO processes including JUN kinase, apoptosis, SMAD/BMP signaling. Scale bar log2 fold change in expression.

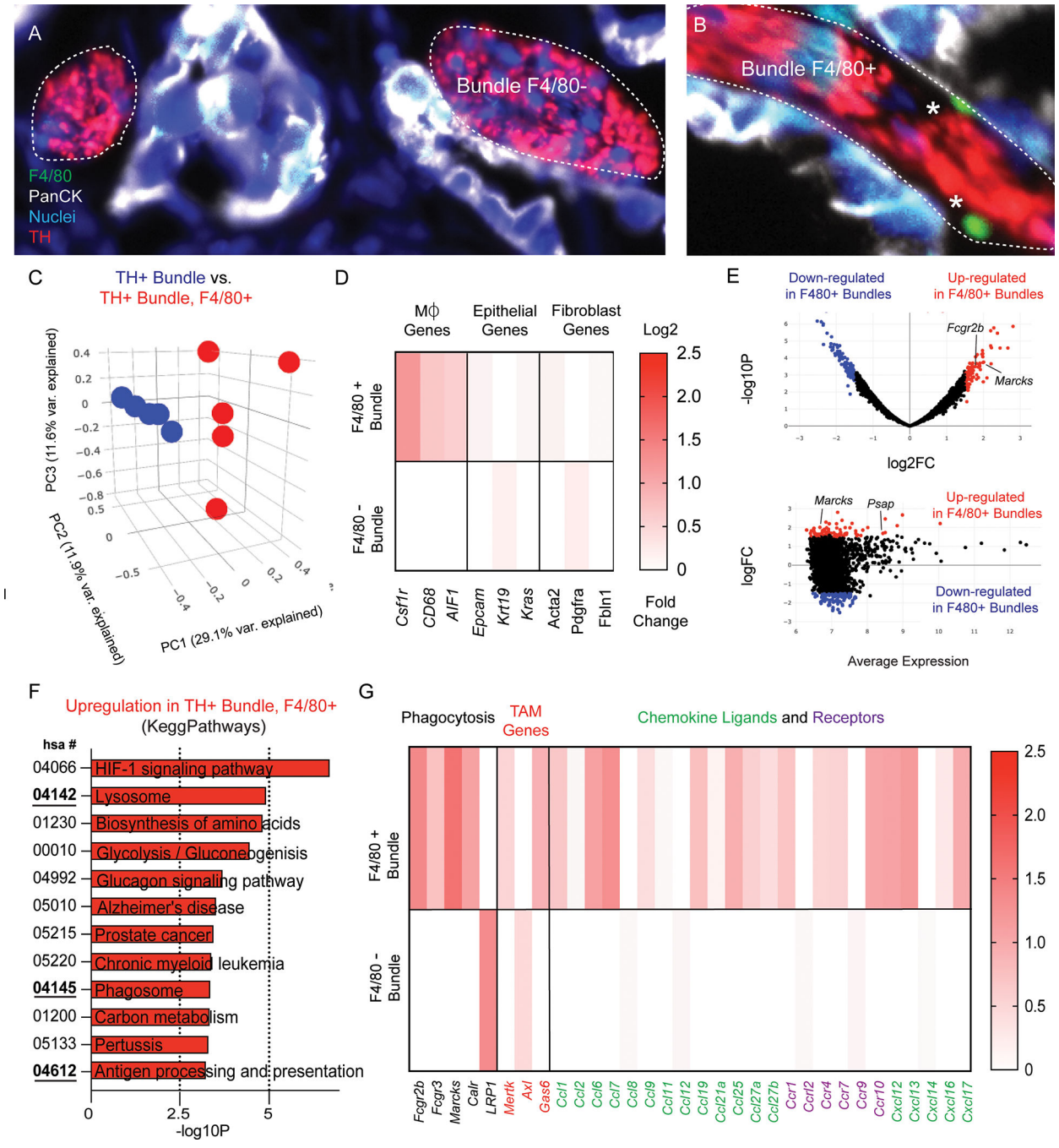

Figure 2. Nerve associated macrophage enriched regions express gene signatures involved in phagocytosis.

Image of TH+ nerve bundles selected for nanostring analysis immunostained for macrophages (F4/80+; green), epithelial cells (PanCK; white), nuclei (blue), tyrosine hydroxylase (TH; red) (A) without F4/80- and (B) with F4/80+ labeled cells. (C) Principal component analysis of comparing TH+ bundles and TH+ bundles containing F4/80+ cells. 10 total ROI's from N = 5 independent bundles and N = 5 bundle + F4/80 ROI's. (D) Heatmap of differentially expressed genes compared from 10 total ROI's in F4/80 positive and F4/80 negative TH+ bundles in cell type gene clusters (macrophages, fibroblasts,

epithelial). Scale bar represents log2 fold change. (E) Volcano plot and MA plot highlighting significant differential gene expression upregulated (red) and downregulated (blue) in TH+, F4/80+ bundles, as well as the average expression. (F) Gene ontology clustering and Kegg Pathways analysis of the most upregulated pathways based on differential gene expression analysis. (G) Highlighted gene expression changes in gene classes involved in GO processes including phagocytosis, chemokine ligands and receptors, and TAM genes.

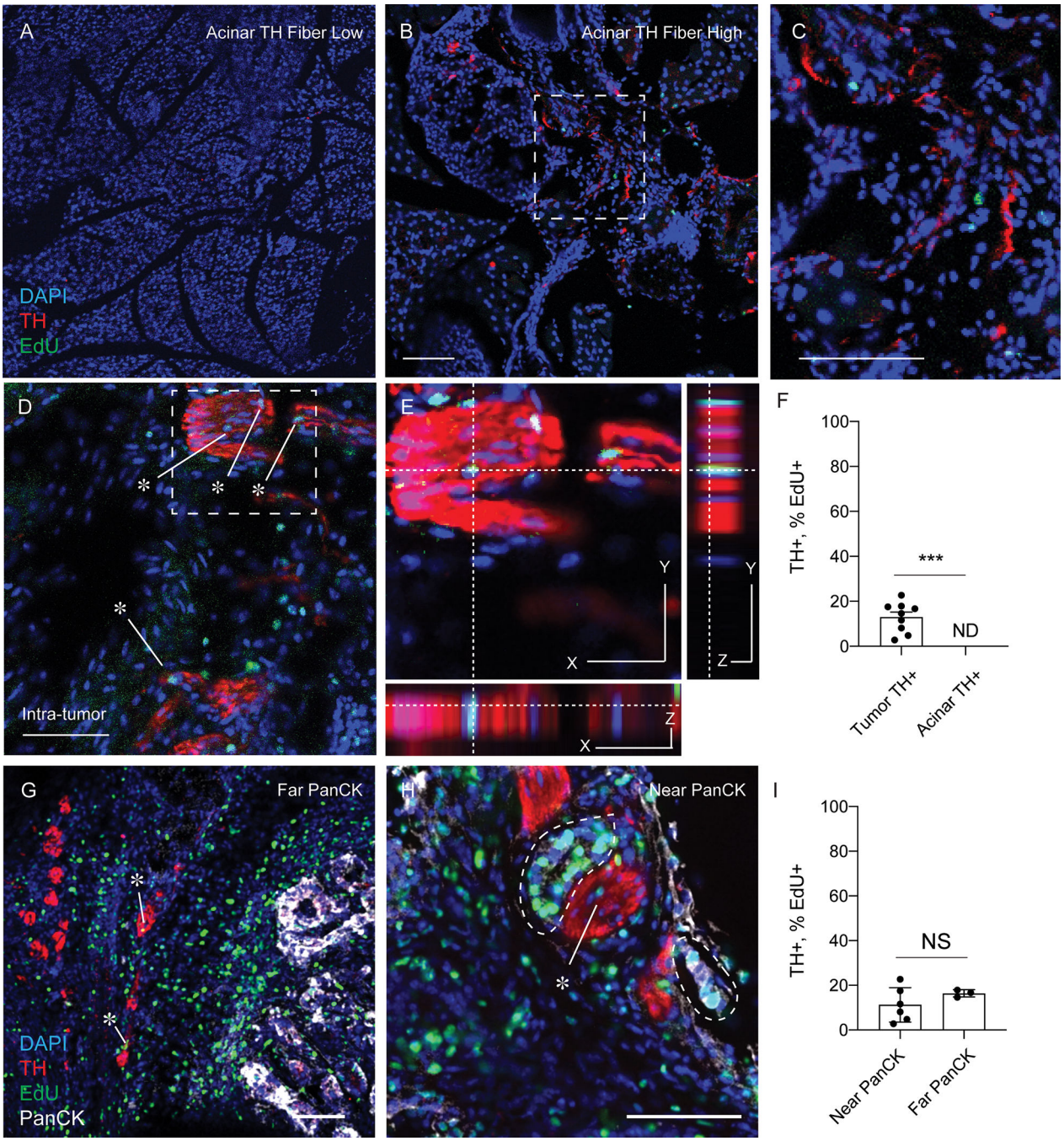

Figure 3. Proliferation of local neuroglia in the tumor nerve microenvironment.

(A) Immunofluorescence of KPC mice injected with EdU, sacrificed prior to any tumor development. Pancreas was stained for DAPI (blue), TH (red) and EdU (green). Images show representative regions with low presence of TH+ fibers and (B) TH+ fiber high regions of pancreas tissue. (D-E) Immunofluorescence of nerve bundles from PDAC tumors from KPC mice stained for DAPI (blue), TH (red), EdU (green) and PanCK (white). (E) High magnifications images for colocalization analysis of EdU+ cells within TH+ Bundles. (F) Quantification of the density of TH fibers in acinar regions and intra-tumoral regions

from KPC mice. N = 9 regions from 3 KPC (G-H) Immunofluorescence of TH nerves, near PanCK epithelial cells (< 50 microns) or far (> 50 microns). Scale bar (50 microns). Unpaired students t-test, *** p-value < .001. (I) Quantification of the percentage of EdU+ percentage of EdU incorporation into cell nuclei within TH+ regions in tumor near PanCK+ or far from PanCK+ cell types. N = 9 total regions from 3 KPC mice stratified into 6 regions near PaNCK+ and 3 not near PanCK+ cell types. Unpaired students t-test was not significant.

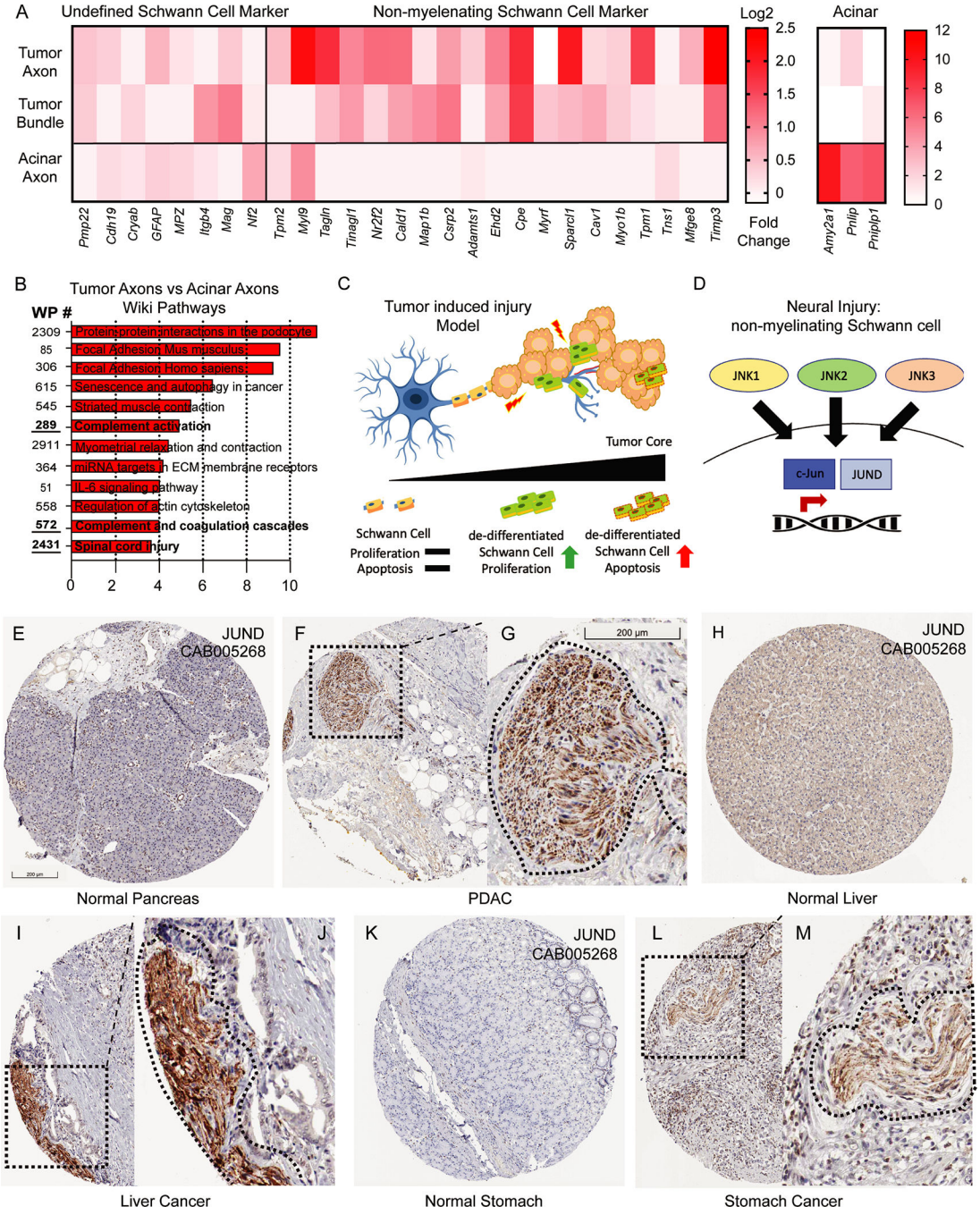

Figure 4. Neural injury and non-myelinating Schwann cell signatures identified in murine transcriptomic analysis are expressed in human PDAC and gastrointestinal tumors.

(A) Gene expression analysis of undefined Schwann cell markers, non-myelinating Schwann cells, and acinar genes from TH+ regions in tumor fibers, bundles and acinar regions. (B) Gene ontology analysis using WikiPathways of the most upregulated pathways based on differential gene expression analysis of TH+ fibers in tumor tissues and TH+ fibers in acinar tissue (C-D) Graphical analysis of tumor injury model and non-myelinating Schwann cell transcriptional activation during neural injury. (E-L) Histological analysis of images containing JUND protein signatures from the Human Protein Atlas (HPA) for multiple

tumor types and their corresponding healthy organ. (E) normal pancreas (F) PDAC low magnification (G) PDAC high magnification (H) liver (I-J) liver cancer (K) stomach (L-M) stomach cancer (Dotted box denotes low magnification while dotted line denotes nerve contour. Scale bar (200 um) in figure E applies to F, H, I, L, Scale bar in figure G applies to J, M.

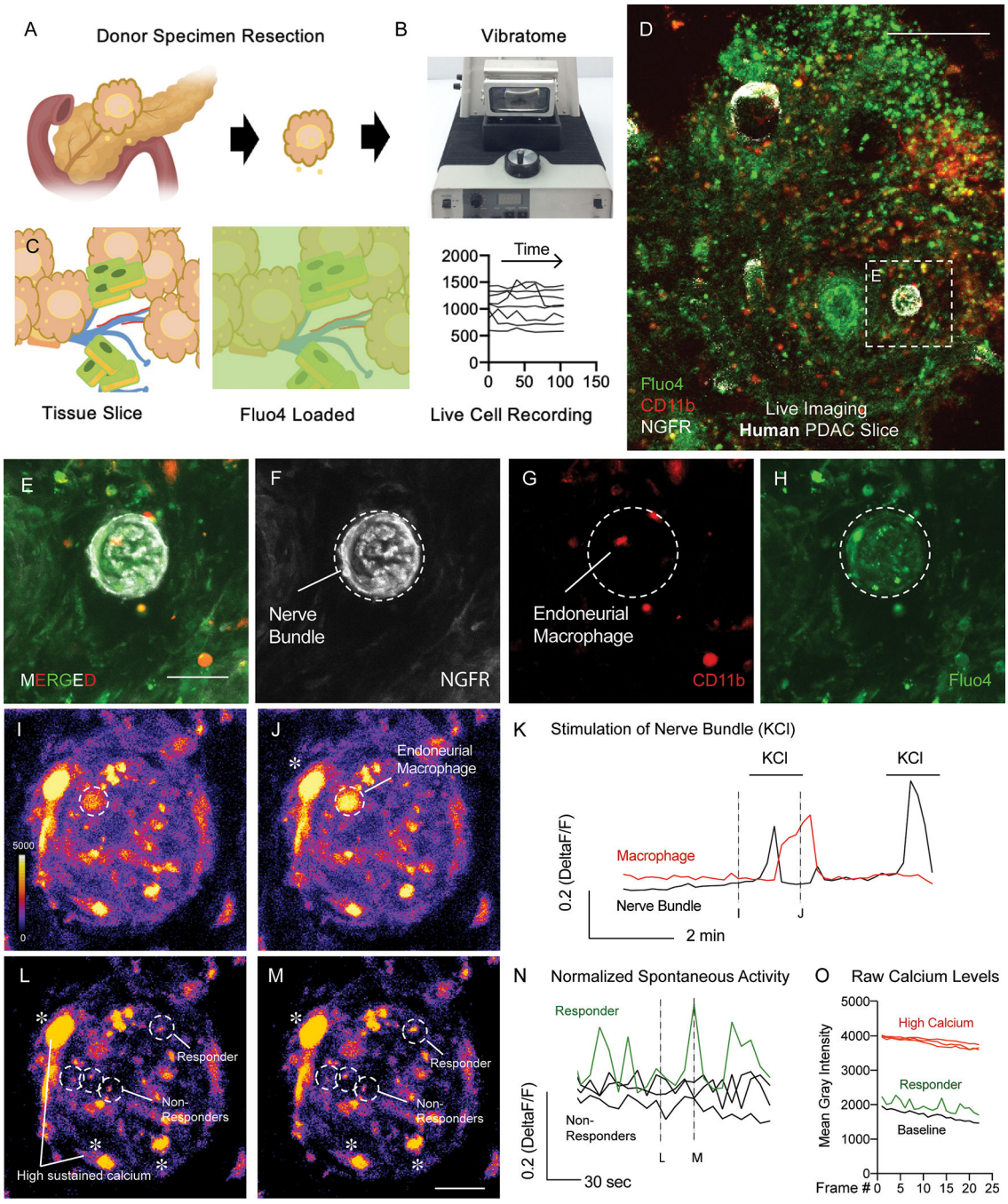

Figure 5. Functional imaging of the tumor nerve microenvironment using organotypic tumor slices from human PDAC donor resections.

(A-C) Graphical representation of cutting and loading organotypic tumor slices with Fluo-4 Ca^{2+} imaging dye to produce live cell recordings. (D) Loaded PDAC tumor slices using *in-situ* cytolabeling to identify regions containing NGFR+ tumor bundles, CD11b+ immune cells, and Fluo-4 loaded cell types. Scale bar 200 microns (upper right). (E-H) Still frame high magnification images recordings of nerve bundles with (E) merged fluorescent channels and (F) split channel views of containing NGFR+ bundles, (G) CD11b+ immune cells, (H) Fluo-4 labeled cells. Scale bar 30 microns (bottom right). (I) Pseudocolor scale

of nerve bundles (I) before and (J) after stimulation of nerve axons using KCl. Pseudocolor scale bar for Ca^{2+} levels shown in I (bottom left). (K) Raw traces of live cell recordings of an endoneural CD11b+ immune cell during KCl stimulation. (L-M) Still frame images of live recordings of spontaneous activity of cell activity within NGFR+ labeled nerve bundles. Scale bar in I applies to L and M. (N) Raw traces of live cell activity records from responding and non-responding cells. (O) Raw traces of cell types containing high sustained levels of calcium in NGFR+ cells, responding cells, and baseline Ca^{2+} levels. Graph shown as non-normalized calcium levels.